PCCP

PAPER

View Article Online
View Journal | View Issue

Cite this: *Phys. Chem. Chem. Phys.*, 2019, **21**, 23893

Falloff curves and mechanism of thermal decomposition of CF_3I in shock waves†

C. J. Cobos,[a] L. Sölter,[b] E. Tellbach[b] and J. Troe *[bc]

Received 28th August 2019,
Accepted 7th October 2019

DOI: 10.1039/c9cp04771a

rsc.li/pccp

The falloff curves of the unimolecular dissociation CF_3I (+Ar) → CF_3 + I (+Ar) are modelled by combining quantum-chemical characterizations of the potential energy surface for the reaction, standard unimolecular rate theory, and experimental information on the average energy transferred per collision between excited CF_3I and Ar. The (essentially) parameter-free theoretical modelling gives results in satisfactory agreement with data deduced from earlier shock wave experiments employing a variety of reactant concentrations (between a few ppm and a few percent in the bath gas Ar). New experiments recording absorption–time signals of CF_3I, I_2, CF_2 and (possibly) IF at 450–500 and 200–300 nm are reported. By analysing the decomposition mechanism, besides the unimolecular dissociation of CF_3I, these provide insight into the influence of secondary reactions on the experimental observations.

I. Introduction

The thermal decomposition of CF_3I has attracted considerable interest for a number of reasons. On the one hand, it has served as a source of CF_3 radicals in shock waves.[1–3] On the other hand, with its weak C–I bond in the presence of strong C–F bonds, it represents a prototype of a unimolecular dissociation reaction of simple bond-fission character.[4–15] Furthermore, its secondary reactions are related to processes of importance in chemical lasers and laser-induced isotope separation.[16,17] The role of secondary reactions, in flow system studies of CF_3I dissociation up to about 800 K, remained unclear for quite some while. Only shock wave experiments, using iodine atom resonance absorption spectroscopy (ARAS) and employing very low reactant CF_3I concentrations,[13,15] directly led to the rate constant of the unimolecular reaction. Although some modelling of this rate constant in its falloff range had been made in earlier work, only with the ARAS results such modelling could be put on a safe basis.[15] Nevertheless, the theoretical approach to the falloff curves left something to be desired. First, it was based on only simplified versions of Rice–Ramsperger–Kassel–Marcus (RRKM) theory. This approach in the present work is extended by accounting for the finer details of the potential energy surface along the reaction coordinate. Second and more seriously, the average energy $\langle\Delta E\rangle$ transferred per collision between the bath gas M and excited CF_3I (or the equivalent collision efficiency β_c) was only treated as a fit parameter. It was overlooked that $\langle\Delta E\rangle$ (for the bath gas M = Ar) had been measured directly in IR-multiphoton excitation experiments.[18–21] With the background of the mentioned experimental and theoretical studies, it appeared attractive to us to investigate the reaction again and in greater detail. We model the rate constant in terms of loose-activated complex unimolecular rate theory, determining the required molecular parameters by quantum-chemical calculations. After introducing the experimental $\langle\Delta E\rangle$, falloff curves are constructed and expressed in the form recommended in ref. 22 and 23. The influence of uncertainties in the C–I bond energy is also investigated. Finally, a comparison with the ARAS shock wave results is made.

Having established reliable falloff curves, new shock wave experiments were performed using alternatives to the ARAS detection method. While the ARAS experiments used reactant concentrations as low as 1–4 ppm of CF_3I in Ar[15] (or in Kr[13]), the present work employs mixtures with 100–1500 ppm (mostly about 500 ppm). The present experiments were able to monitor CF_3I concentrations with considerably reduced reactant concentrations in comparison to earlier shock tube work (employing reactant concentrations of 0.5–5%[6,9,14]). Within the present range of reactant concentrations, the onset of secondary reactions can be monitored. Insight into the complex thermal decomposition mechanism is obtained with the help of absorption spectroscopy in the ranges 200–300 and 450–500 nm. On the basis of the detailed reaction mechanism (being probably still incomplete), the previous high-concentration shock wave experiments could also be reinterpreted. Finally, the identification of species with so far unknown high-temperature absorption coefficients

[a] *INIFTA, Facultad de Ciencias Exactas, Universidad Nacional de La Plata, CONICET, Casilla de Correo 16, Sucursal 4, La Plata (1900), Argentina*
[b] *Institut für Physikalische Chemie, Universität Göttingen, Tammannstrasse 6, D-37077 Göttingen, Germany. E-mail: jtroe@gwdg.de*
[c] *Max-Planck-Institut für Biophysikalische Chemie, Am Fassberg 11, D-37077 Göttingen, Germany*

† Electronic supplementary information (ESI) available: (1) Modelling of rate constants and (2) modelling of spectral properties. See DOI: 10.1039/c9cp04771a

was facilitated by quantum-chemical calculations of oscillator strengths.

II. Modelling of dissociation rate constants

Our modelling of rate constants for the unimolecular dissociation of the C–I bond in CF_3I, first, focussed on the properties of the minimum-energy path (MEP) potential $V(r)$ of the reaction and the change of transitional mode quanta $\nu(r)$ along the MEP reaction coordinate r. $V(r)$ and $\nu(r)$ were derived by quantum-chemical calculations. A 6-311G(d) basis set for I atoms as tabulated in ref. 24 and 25 and a 6-311+G(3df) basis set for C and F atoms were employed. With these basis sets optimized structures and vibrational frequencies were calculated at the M06-2X level (for details of our approach, see *e.g.* ref. 26–30; more details are given in the ESI†). $V(r)$ (computed at the CCSD(T)//M06-2X level) could be approximated using a Morse function (with the Morse parameters $\beta \approx 1.45$ Å^{-1}, $r_e \approx 2.16$ Å, and $D_e = 225.9$ kJ mol^{-1}). The transitional mode quanta $\nu(r)$ were found to decay exponentially along the MEP (with decay parameters $\alpha \approx 0.59$ and 0.61 Å^{-1}, such that the ratio α/β is not far from the "standard value" $\alpha/\beta \approx 0.5$[31]). The calculation of the rotational contributions requires the determination of centrifugal maxima along the MEP. This was done with the r-dependence of the rotational constant of CF_3I (being approximated using $(B + C)/2 \approx 0.0505\ \text{cm}^{-1}/[1 + 0.551(r - 2.16\ \text{Å}) + 0.138(r - 2.16\ \text{Å})^2]$). Graphical representations of $V(r)$, $\nu(r)$, and $(B + C)/2$ for the CF_3–I bond are given in Fig. S1–S3 of the ESI.†

The pseudo-first order rate constant k_1 of the unimolecular dissociation $CF_3I \rightarrow CF_3 + I$ is expressed in its usual form $k_1/k_{1,\infty} = [x/(1 + x)]F(x)$, with $x = k_{1,0}/k_{1,\infty}$ (the limiting low-pressure rate constant $k_{1,0}$ being proportional to the bath gas concentration [M] = Ar, while the limiting high-pressure rate constant $k_{1,\infty}$ is independent of [M]; $F(x)$ denotes a suitable "broadening factor", see below).

With the information obtained and using the statistical adiabatic channel model (in its classical trajectory version, SACM/CT, from ref. 32), limiting high-pressure rate constants

$$k_{1,\infty} = 5.9 \times 10^{15}(T/1000\ \text{K})^{-2.2}\exp(-28\,930\ \text{K}/T)\ \text{s}^{-1} \quad (1)$$

were derived (for a value of the reaction enthalpy at 0 K of $\Delta H_0^\circ = 224.7$ kJ mol^{-1}[33]). Using $\langle \Delta E \rangle/hc \approx -100$ cm^{-1} independent of temperature, such as that determined experimentally for M = Ar in ref. 21, and employing the formalism of ref. 34, limiting low-pressure rate constants

$$k_{1,0} = [\text{Ar}]5.4 \times 10^{21}(T/1000\ \text{K})^{-10.5}\exp(-31\,360\ \text{K}/T)\text{cm}^3\ \text{mol}^{-1}\ \text{s}^{-1} \quad (2)$$

were calculated (the given value of $\langle \Delta E \rangle$ between 750 and 2000 K corresponds to the collision efficiency $\beta_c \approx 0.076(1000\ \text{K}/T)^{1.2}$, see the ESI†). The construction of falloff curves following ref. 22 and 23, furthermore, requires information on center broadening factors of the falloff curves $F_{cent} = F(x = 1)$.[34] These were derived with the method proposed in ref. 23 and 35 (leading to $F_{cent} = 0.20$, 0.16, 0.14, and 0.14 at T/K = 750, 1000, 1500, and 2000, respectively). Fig. 1 shows the corresponding falloff curves for selected temperatures. The latter were chosen to be 950, 1050, and 1200 K, in order to compare with the modelling from ref. 15 (which used variational RRKM theory for $k_{1,\infty}$, while $k_{1,0}$ was derived following ref. 34 with an assumed $\beta_c \approx 100\ \text{K}/T$ and $F_{cent} = 0.188$). Fig. 1 shows that the limiting values of the present falloff curves differ considerably from those of ref. 15. The figure also includes experimental ARAS results from ref. 15 (the measured points were corrected for slight temperature "mismatch" using the modelled temperature dependence of the rate constants at the given [Ar]). The agreement between the ARAS data and the modelled falloff curves appears quite satisfactory. While the differences in the modelled $k_{1,\infty}$ are only small, larger discrepancies are observed in the modelled limiting low-pressure rate constants $k_{1,0}$. This could be due to differences in several input factors (see the basic formalism from ref. 34). The most probable reason seems to us to be that centrifugal barriers were accounted for in the present work (on the basis of Fig. S3 of the ESI†), while this was not done or done differently in ref. 15. This reduces the rotational factors F_{rot} in $k_{1,0}$. A further analysis of the difference does not appear warranted at this stage.

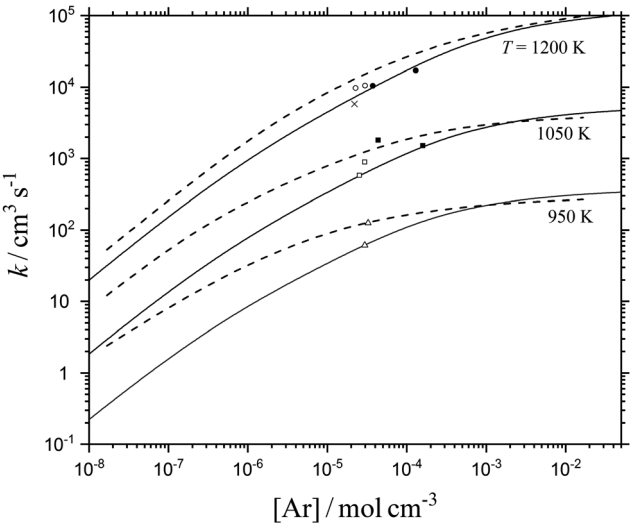

Fig. 1 Falloff curves for the unimolecular dissociation $CF_3I \rightarrow CF_3 + I$ (full lines: modelling from this work (see Section III), dashed lines: modelling from ref. 15; experimental results from this work: ● (1200 K), ■ (1050 K); from ref. 15: ○ (1200 K), □ (1050 K), Δ (950 K); from ref. 8: × (1200 K, reevaluated); influence of secondary reactions in the present work and in ref. 8 accounted for: see Section III).

We also inspected the influence of uncertainties in the reaction enthalpy. Increasing ΔH_0° by 4 kJ mol^{-1} decreases k_1 (at [Ar] = $(5 \times 10^{-5}$–$1.5 \times 10^{-4})$ mol cm^{-3}) by a factor of 1.5–2 (decreasing ΔH_0° by 4 kJ mol^{-1} increases k_1 by the same factor). Measurements and modelled (unadjusted) falloff curves, therefore, agree better than this uncertainty and confirm the validity of the thermochemistry used in the literature.[33,36,37] Nevertheless, the finer details of the shape of the falloff curves should also be noted. In particular, different approaches of k_1 toward the

limiting low- and high-pressure rate constants ($k_{1,0}$ and $k_{1,\infty}$, resp.) are to be accounted for when the more recent falloff expressions from ref. 22 and 23 are used instead of the older forms from ref. 34. The modelling of the falloff curves and their comparison with the ARAS results from ref. 15 in the foregoing section has been described in detail, because it forms the basis for an analysis of the decomposition mechanism under conditions of higher reactant concentrations. This analysis will be made after new experiments are described in the following section.

III. Experimental CF_3I absorption signals

Experiments in the present work were performed in incident and in reflected shock waves in the bath gas Ar. The progress of reaction was followed by recording absorption–time profiles at selected wavelengths in the ranges 200–300 nm and 450–500 nm. Details of our experimental technique have been described before and need not be repeated here (see, *e.g.*, ref. 27–30 and 38–40). Our experiments used reaction mixtures prepared in large mixing vessels before being introduced into a shock tube. Mixtures of CF_3I (99% purity, from Sigma-Aldrich) and Ar (99.9999% purity, from Air Liquide) with reactant concentrations between about 100 and 1500 ppm of CF_3I in Ar (mostly about 500 ppm) were employed. The chosen concentrations are of importance for the analysis of the dissociation mechanism, see below.

In the first part of our experiments we followed the progress of reaction by monitoring the concentration of the decomposing CF_3I, recording absorption signals near the absorption maximum at 271 nm.[6] Two examples of the recorded absorption–time profiles are shown in Fig. 2 and 3. The absorption increases abruptly at the arrival of the incident shock, marked by the first Schlieren peak. The second Schlieren peak indicates the arrival of the reflected shock. The second absorption rise then is followed by the decay of the CF_3I absorption due to reaction. The evaluation of the signals requires careful reconstruction of the room temperature absorption level before the arrival of the incident shock. One also has to reconstruct the absorption level

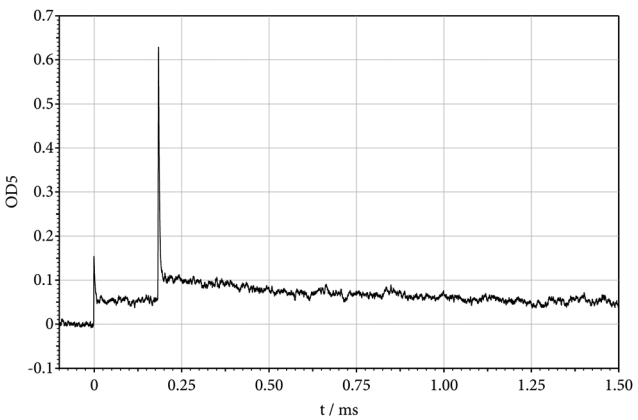

Fig. 2 Absorption–time profile of decomposing CF_3I, recorded at 271 nm (532 ppm of CF_3I in Ar, T = 1031 K, [Ar] = 1.56 × 10^{-4} mol cm^{-3}).

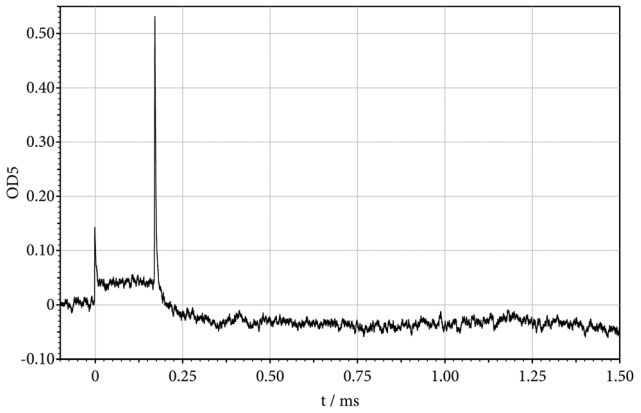

Fig. 3 As Fig. 2, but at higher temperatures (536 ppm of CF_3I in Ar, T = 1219 K, [Ar] = 1.27 × 10^{-4} mol cm^{-3}).

directly behind the reflected shock in order to separate the absorption step and Schlieren peak. These operations could be done with the help of the temperature-dependent absorption coefficients of CF_3I determined in ref. 6 and 41. Finally, the zero-absorption line also had to be reconstructed. A temperature of 622 K behind the incident shock in Fig. 2 is too low to produce substantial dissociation of CF_3I before the arrival of the reflected shock. At a temperature of 1030 K behind the reflected shock, however, the dissociation of CF_3I sets in. It is important to note that the dissociation is not complete within the observation time of about 1.3 ms. This is of relevance when the reaction mechanism is considered in more detail, see below. It is also important to note that the disappearance of CF_3I in Fig. 2 and 3 considerably slows with increasing reaction time and does not reach the zero-absorption line.

The initial rate of CF_3I disappearance was represented by a first-order rate law,

$$[CF_3I] \approx [CF_3I]_{t=0}\exp(-kt) \quad (3)$$

with an apparent rate constant k. Experimental values of k were derived from reflected shocks (for [Ar] larger than 10^{-4} mol cm^{-3}) and from incident shocks (for [Ar] in the range of (2–4) × 10^{-5} mol cm^{-3}). In spite of the similarity of the recorded signals shown in Fig. 2 and 3 to the signal reported in ref. 8 (for 20 times larger $[CF_3I]_{t=0}$), it is by no means clear that the apparent initial rate constant k corresponds to the rate constant k_1 for the unimolecular dissociation of CF_3I. This interpretation requires further analysis of the decomposition mechanism given below.

The thermal decomposition of CF_3I traditionally has been discussed in terms of the reactions summarized in Table 1. For the high-temperature conditions of the present work, a number of aspects are important to note. First, the reverse reactions of all reactions have to be included (this was done here with equilibrium constants from the tabulations in ref. 33). Second, information on the two primary secondary reactions of I (reaction (R2)) and CF_3 (reaction (R4)) with CF_3I is needed. As this is available only for low temperatures,[12,42–44] the corresponding rate constants k_2 and k_4 here were treated as uncertain

Table 1 Mechanism of the thermal decomposition of CF_3I (notes: (a) k_1 = $4.0 \times 10^{12}\exp(-22\,790\ K/T)\ s^{-1}$ modelled with $\Delta H_0^\circ = 224.7\ kJ\ mol^{-1}$ for [Ar] ≈ 1.5×10^{-4} mol cm^{-3} over the range 1000–1050 K; (b) reverse reaction: equilibrium constant from ref. 33; (c) $k_2 = 7.6 \times 10^{12}\exp(-9500\ K/T)\ cm^3\ mol^{-1}\ s^{-1}$ for 400–900 K, from ref. 42–44; (d) k_3 = [Ar]$8.8 \times 10^{13}\exp(-14\,950\ K/T)\ s^{-1}$ for 1080–1570 K and [Ar] = (0.3–1) × 10^{-6} mol cm^{-3}, from ref. 45 and 46; (e) $k_4 \le 1.2 \times 10^8\ cm^3\ mol^{-1}\ s^{-1}$ for 300 K, from ref. 16; (f) $k_{-5} \le 1.2 \times 10^{13}\ cm^3\ mol^{-1}\ s^{-1}$ for 1200 K and [Ar] = 10^{-4} mol cm^{-3} from ref. 47–49)

Number	Reaction	Notes
R1	$CF_3I \rightarrow CF_3 + I$	a, b
R2	$I + CF_3I \rightarrow I_2 + CF_3$	c, b
R3	$I_2 + Ar \rightarrow 2I + Ar$	d, b
R4	$CF_3 + CF_3I \rightarrow C_2F_6 + I$	e, b
R5	$CF_3 + CF_3 \rightarrow C_2F_6$	f, b

parameters and their influence was investigated. k_3 was taken unchanged from ref. 45 and k_5 from ref. 39. Simulating the kinetics of the reactions given in Table 1 leads to concentration–time profiles of CF_3I such as those shown in Fig. 4. The plot of $[CF_3I]/[CF_3I]_{t=0}$ as a function of k_1t well reproduces the experimentally observed slowing of the CF_3I decomposition rate with time t. It is essential not to increase the fitted rate constant k_1 beyond the given value because this would strongly reduce the overall yield of the reaction (a decrease of k_{-1} on the other hand would have no influence). An increase of k_2 by a factor of 10 reduces the calculated half-life of CF_3I by only 4% while an increase of k_4 by a factor of 10 has an even smaller effect. The concentration–time profiles of CF_3I thus are unsuitable for fitting k_2 and k_4. Extracting k_1 from the CF_3I profiles, however, required accounting for the slowing of the decomposition. As the $[CF_3I]/[CF_3I]_{t=0}$ profile as a function of k_1t hardly varies with temperature (see Fig. 4), the profile shown in Fig. 4 could be used for extracting k_1 from the initial rate constant k of eqn (3) or, better,

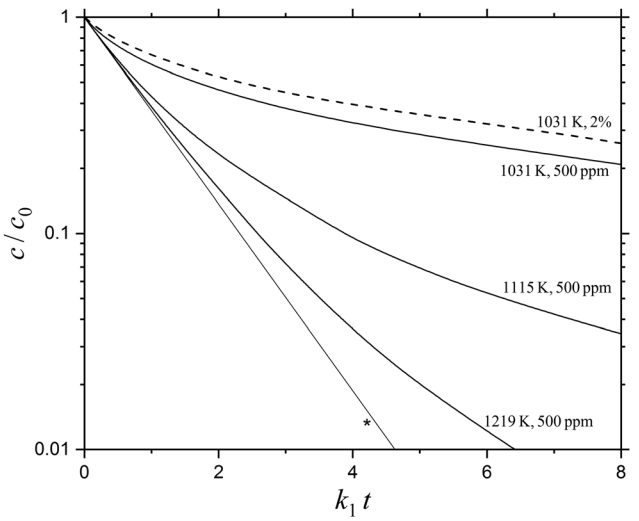

Fig. 4 Kinetics simulation of CF_3I concentration–time profiles (c = $[CF_3I]$, c_0 = $[CF_3I]_{t=0}$, full lines: simulation with reactions of Table 1 for 500 ppm of CF_3I in Ar, dashed line: for 2% of CF_3I in Ar; *: profile without secondary reactions, k_1 = rate constant for unimolecular dissociation of CF_3I, t = time, see Section III).

Table 2 Experimental rate constants k_1 for the unimolecular dissociation $CF_3I \rightarrow CF_3 + I$ (present work, evaluated with the reaction mechanism of Section III)

T/K	[Ar]/mol cm^{-3}	k_1/s^{-1}
1005	3.2×10^{-5}	5.5×10^2
1031	1.6×10^{-4}	6.0×10^2
1045	6.5×10^{-5}	1.3×10^3
1076	5.8×10^{-5}	4.5×10^3
1130	5.7×10^{-5}	6.5×10^3
1152	2.5×10^{-5}	5.6×10^3
1160	1.4×10^{-4}	1.3×10^4
1195	9.0×10^{-5}	7.8×10^3
1219	1.3×10^{-4}	2.5×10^4
1220	1.3×10^{-4}	2.0×10^4

from a fit of the complete measured CF_3I profile to the kinetics simulation. The resulting k_1 values are summarized in Table 2. Selected values are included in Fig. 1 and compared with the ARAS data from ref. 15 and the modelled falloff curves. All data are consistent with each other. Increasing the reactant concentration from the 532 ppm of Fig. 2 and 3 to the 2% in ref. 8 has a noticeable effect: it increases the CF_3I half-life by a factor of 1.6. The correspondingly reevaluated value is included in Fig. 1; it agrees well with the other results shown (the agreement with the data from ref. 6 is less satisfactory, because full CF_3I profiles were not reported in ref. 6).

Although the measured CF_3I absorption–time profiles of the present work appear consistent with the modelling of k_1, additional measurements of I_2 signals as described in the following section raise questions, suggesting that further reactions need to be considered. At this moment it appears uncertain whether they have an influence on kinetics simulations of CF_3I profiles such as those shown in Fig. 4. Because the agreement of experimental and modelled k_1 values in Fig. 1 looks satisfactory, one is tempted to assume that this is not the case.

IV. Experimental I_2 absorption signals

The simulation of the CF_3I profiles described in Section III indicated that conclusions on the rate constants k_2 and k_4 of reactions (R2) and (R4) could be drawn only to a limited extent, while the CF_3I profiles independent of uncertainties in the mechanism led to k_1. In order to learn more about k_2 and k_4, profiles of intermediate reaction species should be measured. Information on CF_3-profiles would be difficult to obtain, because the absorption coefficient of this intermediate in the investigated spectral range (at wavelengths larger than 200 nm) is only a small value.[50] We have, furthermore, extended the measurements of absorption coefficients of CF_2 to wavelengths near 200 nm (CF_2 prepared by the thermal decomposition $CHF_3 \rightarrow CF_2 + HF$,[38] see also ref. 27 and 51). We found that CF_2 (from reactions not included in Table 1) or the strong absorber CF (which forms at considerably higher temperatures in the thermal decomposition of CF_2[40]) would not contribute to absorption signals of the present work. In contrast to this, I_2 should be detectable, either in the intense Cordes bands near 200 nm or in the visible range 450–500 nm. Fig. 5 and 6 show

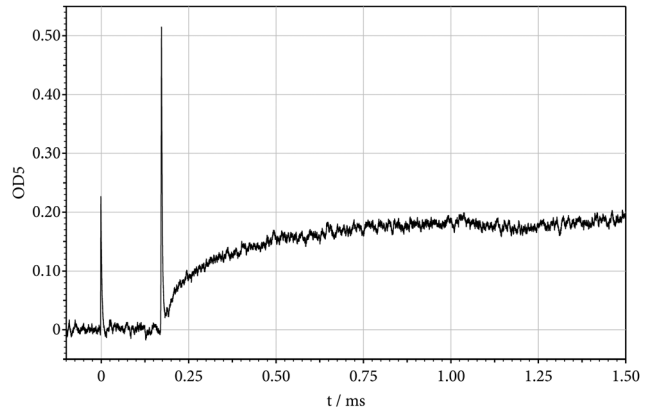

Fig. 5 Absorption signal recorded at 487 nm during the thermal decomposition of CF_3I (1485 ppm of CF_3I in Ar, T = 1197 K, [Ar] = 1.25 × 10^{-4} mol cm^{-3}, see Section IV).

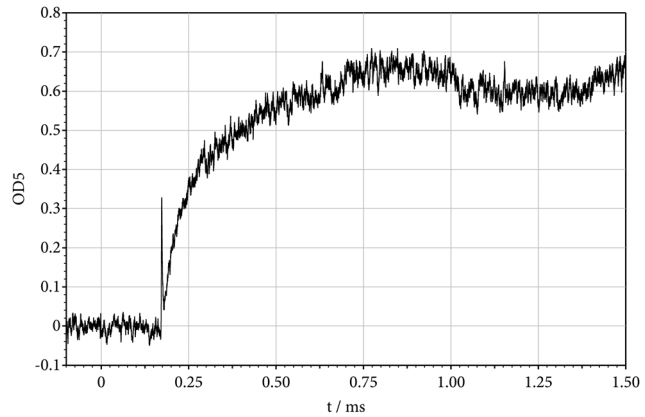

Fig. 6 Absorption signal recorded at 200 nm during the thermal decomposition of CF_3I (529 ppm of CF_3I in Ar, T = 1188 K, [Ar] = 1.31 × 10^{-4} mol cm^{-3}, see Section IV).

examples for 200 and 487 nm under similar experimental conditions. While the I_2 absorption coefficients at 487 nm are observed under shock wave conditions,[45,46] they are observed near 200 nm only at near room temperature.[51–54] Fig. 5 and 6 show the absorption signals from I_2, one then could calibrate the high temperature absorption coefficients of I_2 near 200 nm against those from 450 to 500 nm. However, this procedure faces the following problem. Fig. 7 shows an absorption signal at 487 nm for conditions close to those of Fig. 2. The kinetics simulation predicts a profile such as that included in Fig. 7. This considerably differs from the observations. Furthermore, absorption signals at the wavelengths of Fig. 5–7 were still observable at temperatures in the range of 1300–1600 K where I_2 should have disappeared by thermal decomposition (at even higher temperatures these signals finally disappeared). Apparently besides I_2 an additional species must have contributed to the signals shown in Fig. 5–7 and it has similar spectral properties to I_2, but is thermally more stable. Quantum-chemical calculations of oscillator strengths (for IF, I_2, CF, CFI, CF_2I, CF_3I, and CF_2, see the ESI†) indicated that this can only be IF. This species is thermally more stable than I_2 (dissociation enthalpy

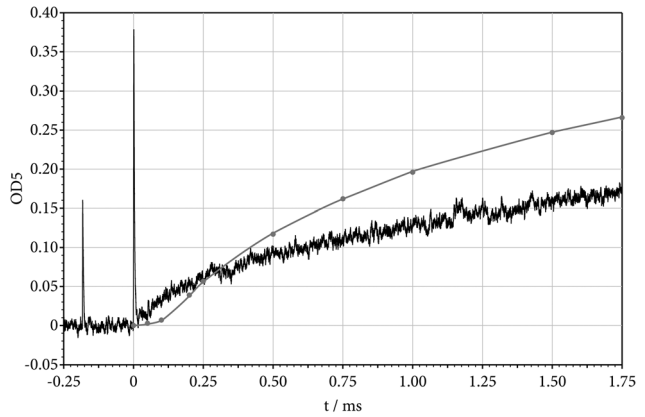

Fig. 7 Absorption signal recorded at 487 nm during the thermal decomposition of CF_3I in comparison to the simulated I_2 profile (1485 ppm of CF_3I in Ar, T = 1048 K, [Ar] = 1.49 × 10^{-4} mol cm^{-3}, t = 1 ms corresponds to $t = 1.441/k_1$ from Section III).

$\Delta H_0^\circ = 277.3$ kJ mol^{-1} for IF instead of 148.8 kJ mol^{-1} for I_2[33]). Its calculated oscillator strength is even larger than that of I_2 in the range of the visible spectrum (see the ESI†). Unfortunately, so far only information from the emission spectra of IF at 450–650 nm is available (see, *e.g.* ref. 55 and 56), but this looks consistent with the present identification of the additional species. IF might be formed in the reaction

$$I + CF_3 \rightarrow IF + CF_2 \qquad (R6)$$

followed by reactions consuming CF_2 and the dissociation of IF. An alternative could be a second, high energy, dissociation channel of CF_3I leading to CF_2 + IF. A problem might be seen in the endothermicity of reaction (R6), with $\Delta H_0^\circ = 85.0$ kJ mol^{-1}.[33] However, this appears not to be too relevant for the high temperatures of the present work. Nevertheless, our identification of an additional absorber in Fig. 5–7 remains uncertain, such that more work is required here.

V. Conclusions

After analysis of the decomposition mechanism of CF_3I, the recorded absorption–time profiles of CF_3I of the present work lead to rate constants for the unimolecular dissociation of CF_3I. Within the experimental uncertainty of the C–I bond energy, experiments with various reactant concentrations and different detection methods are in agreement with the theoretically modelled rate constants. The latter confirm that all experiments correspond to the central part of the falloff curves of the unimolecular dissociation. Implementing experimental information on collisional energy transfer of vibrationally highly excited CF_3I[18–21], the modelling then is essentially free from adjustable parameters. In this respect, the present work goes beyond the usual modelling of other unimolecular reaction rate constants.

The present work also provides evidence for the intermediate formation of a species with larger thermal stability than I_2 but having similar spectral features. Tentatively this species is

identified to be IF. The importance of various secondary reactions of the decomposition was discussed, but for definite conclusions we need to wait for a confirmation of the identity of IF. The comparison of the present theoretical modelling of falloff curves for CF_3I dissociation with that from ref. 15 showed major differences in the extrapolated limiting low-pressure rate constants. Our detailed analysis such as that described in the ESI† proposes that this is due to the exclusion of centrifugal barriers in ref. 15.

Conflicts of interest

There are no conflicts to declare.

Acknowledgements

Discussions of this work with K. Hintzer and A. Thaler, technical help by A. I. Maergoiz, and financial support from the Deutsche Forschungsgemeinschaft (Project TR 69/21-1) are gratefully acknowledged.

References

1 A. P. Modica and S. J. Sillers, Experimental and Theoretical Kinetics of High-Temperature Fluorocarbon Chemistry, *J. Chem. Phys.*, 1968, **48**, 3283–3289.
2 N. K. Srinivasan, M.-C. Su, J. V. Michael, A. W. Jasper, S. J. Klippenstein and L. B. Harding, Thermal Decomposition of CF_3 and the Reaction of CF_2 + OH → CF_2O + H, *J. Phys. Chem. A*, 2008, **112**, 31–37.
3 C. J. Cobos, A. E. Croce, K. Luther and J. Troe, Shock Wave Study of the Thermal Decomposition of CF_3 and CF_2 Radicals, *J. Phys. Chem. A*, 2010, **114**, 4755–4761.
4 O. B. Danilov, V. V. Elagin, V. Y. Zalesskii and I. L. Yachnev, Thermal Dissociation of Trifluoroiodomethane, *Kinet. Katal.*, 1975, **16**, 302–305.
5 V. Yu. Zalesskii, A. M. Kokushkin and I. L. Yachnev, Pyrolysis of Perfluoroalkyliodide Vapor in UV Irradiation, *Sov. Phys. Tech. Phys.*, 1977, **22**, 1273–1276.
6 L. Brouwer and J. Troe, Shock Wave Study of the UV Spectrum of CF_3I, *Chem. Phys. Lett.*, 1981, **82**, 1–4.
7 G. A. Skorobogatov, Rate Constant of Thermal Dissociation of Gaseous Trifluoromethyl Iodide, *Kinet. Katal.*, 1982, **23**, 18–21.
8 K. Saito, Y. Yoneda, H. Tahara, S. Kidoguchi and I. Murakami, The Thermal Decomposition of CF_3I in Ar, *Bull. Chem. Soc. Jpn.*, 1984, **57**, 2661–2662.
9 I. S. Zaslonko, Y. I. Mukossev, G. A. Skorobogatov and S. V. Slinkin, Parameters of the Thermal Dissociation of Gaseous CF_3I, *Kinet. Katal.*, 1986, **27**, 734–739.
10 V. Y. Zalesskii, Determination of the Rate Constant for Thermal Dissociation of Molecules by the Shock-Tube Method, *Kinet. Katal.*, 1988, **29**, 528–535.
11 I. S. Zaslonko, Y. K. Mukoseev, G. A. Skorobogatov and V. K. Khripun, Measurement of the Rate Constant for the Thermal Dissociation of Gaseous CF_3I in a Shock Tube, *Kinet. Katal.*, 1989, **31**, 1046–1052.
12 G. A. Skorobogatov, B. P. Dymov and V. K. Khripun, Determination of Rate Constants and Equilibrium Constants of RI = R + I and I + RI = I_2 + R for R = CF_3, C_2F_5, or CF_4F_9, *Kinet. Katal.*, 1991, **32**, 252–259.
13 S. S. Kumaran, M.-C. Su, K. P. Lim and J. V. Michael, Thermal Decomposition of CF_3I using I-Atom Absorption, *Chem. Phys. Lett.*, 1995, **243**, 59–63.
14 J. H. Kiefer and R. Sathyanarayana, Vibrational Relaxation and Dissociation in the Perfluoromethyl Halides, CF_3Cl, CF_3Br, and CF_3I, *Int. J. Chem. Kinet.*, 1997, **29**, 705–716.
15 N. S. Bystrov, A. V. Emelianov, A. V. Eremin and P. I. Yatsenko, Direct Measurements of Rate Coefficients for Thermal Decomposition of CF_3I using Shock-Tube ARAS technique, *J. Phys. D: Appl. Phys.*, 2018, **51**, 1–8.
16 T. I. Andreeva, S. V. Kuznetsova, A. I. Maslov, I. I. Sobel'man and V. N. Sorokin, Investigation of Reactions of Excited Iodine Atoms by Means of a Photodissociation Laser, *Khim. Vys. Energ.*, 1972, **6**, 418–424.
17 C. N. Plum and P. L. Houston, Improved Isotope Separation in Laser Dissociation of Trifluoromethyl Halides: Scavenging of CF_3 with HI, *Appl. Phys.*, 1981, **24**, 143–146.
18 B. Abel, B. Herzog, H. Hippler and J. Troe, Infrared Multiphoton Excitation of CF_3I. I. Transient Ultraviolet Absorption Study of After-Pulse Dissociation and Excited State Populations, *J. Chem. Phys.*, 1989, **91**, 890–899.
19 B. Abel, B. Herzog, H. Hippler and J. Troe, Infrared Multiphoton Excitation of CF_3I. II. Collisional Energy Transfer of Vibrationally Highly Excited CF_3I, *J. Chem. Phys.*, 1989, **91**, 900–905.
20 B. Abel, H. Hippler and J. Troe, Infrared Multiphoton Excitation Dynamics of CF_3I. I. Populations and Dissociation Rates of Highly Excited Rovibrational States, *J. Chem. Phys.*, 1992, **96**, 8863–8870.
21 B. Abel, H. Hippler and J. Troe, Infrared Multiphoton Excitation Dynamics of CF_3I. II. Collisional Effects on Vibrational and Rotational State Populations, *J. Chem. Phys.*, 1992, **96**, 8872–8876.
22 J. Troe and V. G. Ushakov, Revisiting Falloff Curves of Thermal Unimolecular Reactions, *J. Chem. Phys.*, 2011, **135**, 054304.
23 J. Troe and V. G. Ushakov, Representation of "Broad" Falloff Curves for Dissociation and Recombination Reactions, *Z. Phys. Chem.*, 2014, **228**, 1–10.
24 D. Feller, The Role of Databases in Support of Computational Chemistry Calculations, *J. Comput. Chem.*, 1996, **17**, 1571–1586.
25 K. L. Schuchardt, B. T. Didier, T. Elsethagen, L. Sun, V. Gurumoorthi, J. Chase, J. Li and T. L. Windus, Basis Set Exchange: A Community Database for Computational Sciences, *J. Chem. Inf. Model.*, 2007, **47**, 1045–1052.
26 M. J. Frisch, *et al.*, *Gaussian 09, Revision A.02-SMP*, Gaussian Inc., Wallingford, CT, 2009.
27 C. J. Cobos, A. E. Croce, K. Luther, L. Sölter, E. Tellbach and J. Troe, Experimental and Modeling Study of the Reaction C_2F_4 (+M) ↔ CF_2 + CF_2 (+M), *J. Phys. Chem. A*, 2013, **117**, 11420–11429.

28 C. J. Cobos, L. Sölter, E. Tellbach and J. Troe, Shock Wave Study of the Thermal Dissociations of C_3F_6 and c-C_3F_6. I. Dissociation of Hexafluoropropene, *J. Phys. Chem. A*, 2014, **118**, 4880–4888.

29 C. J. Cobos, K. Hintzer, A. Thaler, L. Sölter, E. Tellbach and J. Troe, Shock Wave and Theoretical Modelling of the Dissociation of CH_2F_2. I. Primary Processes, *J. Phys. Chem. A*, 2017, **121**, 7813–7819.

30 C. J. Cobos, G. Knight, L. Sölter, E. Tellbach and J. Troe, Kinetic and Spectroscopic Studies of the Reaction of CF_2 with H_2 in Shock Waves, *J. Phys. Chem. A*, 2017, **121**, 7827–7834.

31 C. J. Cobos and J. Troe, Theory of Thermal Unimolecular Reactions at High Pressures. II. Analysis of Experimental Results, *J. Chem. Phys.*, 1985, **83**, 1010–1015.

32 A. I. Maergoiz, E. E. Nikitin, J. Troe and V. G. Ushakov, Classical Trajectory and Statistical Adiabatic Channel Study of the Dynamics of Capture and Unimolecular Bond Fission. V. Valence Interactions between Linear Rotors, *J. Chem. Phys.*, 1998, **108**, 9987–9998.

33 M. W. Chase, NIST-JANAF Thermochemical Tables, 4th edition, *J. Phys. Chem. Ref. Data, Monogr.*, 1998, **9**, 1–1951.

34 J. Troe, Predictive Possibilities of Unimolecular Rate Theory, *J. Phys. Chem.*, 1979, **83**, 114–126.

35 J. Troe, Theory of Thermal Unimolecular Reactions in the Falloff Range. I. Strong Collision Rate Constants, *Ber. Bunsen-Ges.*, 1983, **87**, 161–169.

36 J. B. Burkholder, J. P. D. Abbatt, R. E. Huie, M. J. Kurylo, D. M. Wilmouth, S. P. Sander, J. R. Barker, C. E. Kolb, V. L. Orkin and P. H. Wine, Chemical Kinetics and Photochemical Data for Use in Atmospheric Studies Evaluation Number 18, JPL Publication 15-10, Jet Propulsion-Laboratory, Pasadena, 2015.

37 E. Goos, A. Burcat and B. Rusic, Extended Third Millenium Ideal Gas and Condensed Phase Thermochemical Database for Combustion with Updates from Active Thermochemical Tables. http://burcat.technion.ac.il/div, September 2005, January 2015.

38 C. J. Cobos, A. E. Croce, K. Luther and J. Troe, Experimental and Modelling Study of the Unimolecular Thermal Decomposition of CHF_3, *Z. Phys. Chem.*, 2011, **225**, 1019–1028.

39 G. Knight, L. Sölter, E. Tellbach and J. Troe, Shock Wave and Modeling Study of the Reaction CF_4 (+M) ↔ CF_3 + F (+M), *Phys. Chem. Chem. Phys.*, 2016, **18**, 17592–17596.

40 C. J. Cobos, G. Knight, L. Sölter, E. Tellbach and J. Troe, Experimental and Modeling Study of the Multichannel Thermal Decomposition of CH_3F and CH_2F, *Phys. Chem. Chem. Phys.*, 2018, **20**, 2627–2636.

41 B. Abel, L. Brouwer, B. Herzog, H. Hippler and J. Troe, Direct Measurement of Near-Threshold Rate Constants for Unimolecular Dissociation of CF_3I after IR Multiphoton Excitation, *Chem. Phys. Lett.*, 1986, **127**, 541–546.

42 S. L. Dobychin, V. I. Mashendzhinov, V. I. Mishin, V. N. Semenov and V. S. Shpak, Kinetics of Thermal Decomposition of Perfluoroalkyl Iodides and D(R-I) Binding Energy, R – CF_3, C_2F_5, n-C_3F_7, iso-C_3F_7, n-C_4F_9, tert-C_4F_9, *Dokl. Akad. Nauk SSSR*, 1990, **312**, 1166–1168.

43 G. S. Laurence, Thermal and Photochemical Exchange of Iodine with Trifluoro-methyl Iodide, *Trans. Faraday Soc.*, 1967, **63**, 1155–1165.

44 J. C. Amphlet and E. Whittle, Reactions of Trifluoromethyl Radicals with Iodine and Hydrogen Iodide, *Trans. Faraday Soc.*, 1967, **63**, 2695–2701.

45 D. Britton, N. Davidson and G. Schott, Shock Waves in Chemical Kinetics. The Rate of Dissociation of Molecular Iodine, *Discuss. Faraday Soc.*, 1954, **17**, 58–68.

46 D. Britton, N. Davidson, W. Gehman and G. Schott, Shock Waves in Chemical Kinetics: Further Studies on the Rate of Dissociation of Molecular Iodine, *J. Chem. Phys.*, 1956, **25**, 804–809.

47 C. J. Cobos, A. E. Croce, K. Luther and J. Troe, Temperature and Pressure Dependence of the Reaction 2 CF_3 (+M) ↔ C_2F_6 (+M), *J. Phys. Chem. A*, 2010, **114**, 4748–4754.

48 G. A. Skorobogatov, V. K. Khripun and A. G. Rebrova, Isochoric Isothermal Pyrolysis of Trifluoroiodomethane: CF_3° Recombination Kinetics, *Kinet. Catal.*, 2008, **49**, 466–473.

49 G. A. Skorobogatov, A. G. Rebrova and V. K. Khripun, Rate Constant of the Recombination CF_3° Radicals in a Gas (He, Ar, N_2, or CF_3I), *Kinet. Catal.*, 2010, **51**, 485–491.

50 K. Glänzer, M. Maier and J. Troe, Shock-Wave Study of the High-Temperature UV Absorption and the Recombination of CF_3 Radicals, *J. Phys. Chem.*, 1980, **84**, 1681–1686.

51 A. P. Modica, Electronic Oscillator Strength of CF_3, *J. Phys. Chem.*, 1968, **72**, 4594–4598.

52 P. Sulzer and K. Wieland, Intensitätsverteilung eines kontinuierlichen Absorptionsspektrums in Abhängigkeit von Temperatur und Wellenzahl, *Helv. Phys. Acta*, 1951, **25**, 653–676.

53 J. A. Myer and J. A. R. Samson, Absorption Cross Section and Photoionization Yield of I_2 between 1050 and 2200 Å, *J. Chem. Phys.*, 1970, **52**, 716–718.

54 A. Saiz-Lopez, R. W. Saunders, D. M. Joseph, S. H. Ashworth and J. M. C. Plane, Absolute Absorption Cross-Section and Photolysis Rate of I_2, *Atmos. Chem. Phys.*, 2004, **4**, 1443–1450.

55 L. G. Piper, W. J. Marinelli, W. T. Rawlins and B. D. Green, The Excitation of IF ($B\,^3\Pi_0^+$) by N_2 ($A\,^3\Sigma_u^+$), *J. Chem. Phys.*, 1985, **83**, 5602–5609.

56 W. J. Marinelli and L. G. Piper, Franck-Condon Factors and Absolute Transition Probabilities for the IF ($B^3\Pi_0^+$ $X^1\Sigma^+$) Transition, *J. Quant. Spectrosc. Radiat. Transfer*, 1985, **34**, 321–330.